

**Strong coupling of light with *A* and *B* excitons in GaN microcavities grown on silicon**I. R. Sellers,\* F. Semond, M. Leroux, and J. Massies  
*CRHEA-CNRS, Rue Bernard Gregory, Parc Sophia Antipolis, Valbonne 06560, France*P. Disseix, A-L. Henneghien, J. Leymarie, and A. Vasson  
*LASMEA, Université Blaise Pascal, Clermont Ferrand II, Les Cézeaux, 63177 Aubière Cedex, France*

(Received 19 July 2005; published 9 January 2006)

We present experimental results demonstrating strong-light matter coupling at low and room temperature in bulk GaN microcavities with epitaxial (Al,Ga)N Bragg mirrors grown on silicon (111). At low temperature, the strong coupling of both the *A* and *B* excitonic features of GaN with the cavity mode is clearly resolved in the microcavity. At room temperature a Rabi energy of 50 meV is observed and well reproduced using transfer-matrix reflectivity calculations describing the interaction of both the *A* and *B* excitonic states with the photonic mode.

DOI: 10.1103/PhysRevB.73.033304

PACS number(s): 78.40.Fy, 78.66.Fd, 81.15.Hi

In recent years there has been intensive research into the field of light-matter interaction in semiconductor microcavities and, in particular, the so-called strong-coupling regime.<sup>1,2</sup> Strong coupling occurs when excitons and photons with the same energy and momentum strongly interact to create quasiparticles, which are neither exciton nor photon, but rather the eigenstates of both. These new states, termed cavity polaritons in analogy to bulk polaritons,<sup>3</sup> have a very low in-plane effective mass around  $k=0$ . This creates a number of interesting physical properties not possible for excitons and photons alone. These properties are very interesting from a fundamental point of view but also offer the possibility of a new generation of parametric optical amplifiers and low-threshold lasers<sup>4</sup> based upon stimulated scattering of polaritons.<sup>5</sup>

Most of the early work on strong light-matter coupling has been performed on the group-III arsenides due to the maturity and high material quality of these systems. However, these materials have both an inherently low excitonic Rydberg and oscillator strength, making it difficult to observe strong coupling at high temperatures due to thermal broadening of the excitons.

To observe strong light-matter coupling at room temperature, the exciton binding energy should be in excess of the thermal energy,  $k_B T$ . In this respect the III-N materials offer an alternative to conventional III-V semiconductors as a result of the large exciton binding energies of these systems.<sup>6</sup> Consequently, III-N materials have significantly larger oscillator strengths, and therefore Rabi energies  $\Omega_{\text{Rabi}}$ , than their III-V counterparts. As a result strong light-matter coupling has now been observed experimentally at both low<sup>7</sup> and room temperature in nitride<sup>8,9</sup> microcavities. Indeed, recently we published evidence of strong coupling with a large  $\Omega_{\text{Rabi}}$  of 60 meV at room temperature from a simple, low-finesse, planar GaN microcavity.<sup>8</sup>

In this paper we present a bulk  $\lambda/2$  GaN microcavity grown by molecular beam epitaxy (RIBER Compact 21) on a seven-period epitaxial AlN/Al<sub>0.2</sub>Ga<sub>0.8</sub>N distributed Bragg reflector (DBR) grown directly on silicon (111). The complete growth technique of (0001)-oriented nitrides on silicon is described elsewhere.<sup>10</sup> An indication of the high quality of

the DBR layers is demonstrated by a surface roughness of 0.5 nm over a  $3\text{-}\mu\text{m}^2$  surface area. As a result of this low surface roughness, well-developed terraces and monolayer step edges following the crystallographic axis are observed in large-area atomic force microscopy images. A normal incidence reflectivity of 85% and stop-band width of 450 meV were measured experimentally for the Bragg mirror. After the growth of the GaN active layer on the DBR, the microcavity structure was completed with the deposition of a 10-nm transparent aluminum mirror. It should be mentioned here that a crack density of  $100/\text{mm}^2$  was observed by optical microscopy; however, there is no evidence to suggest that these cracks influence the optical performance of the structure.

Figure 1(a) shows the experimental reflectivity spectra of the microcavity for various angles of incidence from  $5^\circ$  to  $60^\circ$  at 5 K for TE polarization. At the bottom of Fig. 1(a) is shown the photoluminescence (PL) spectrum at 5 K measured prior to the deposition of the aluminum film. The PL emission peaks at 3.51 eV which is high in comparison to conventional  $\mu\text{m}$ -thick GaN on silicon, which typically emits at  $\sim 3.46$  eV at low temperature.<sup>10</sup> This high emission energy results from the large biaxial compressive strain (estimated to  $\sim -4 \times 10^{-3}$ ) within the  $\lambda/2$  GaN layer ( $\sim 66$  nm thick) and is due to the AlN/(Al,Ga)N DBR upon which it is grown. The full width at half maximum (FWHM) of the PL is 19 meV at 5 K. With increasing temperature, the luminescence linewidth increases progressively up to 42 meV at room temperature. Actually, it is known that in nominally undoped GaN, the PL spectra are dominated by donor bound exciton recombination ( $D^0X$ ) at low temperature while, with increasing  $T$ , contributions of *A* and *B* excitons progressively dominate.<sup>11</sup> At room temperature, the PL linewidth reflects emission from both *A* and *B* excitons and a contribution from the thermal tail of their optical phonon replica.<sup>11</sup> Meanwhile, it is also known that in compressively strained GaN, the  $D^0X$  line is linked to the *A* line, with a constant energy separation of 6 meV.<sup>12</sup> The inhomogeneous broadening in GaN arises mainly from strain inhomogeneities, which for simplicity can be considered as both in plane, due to structural defects as

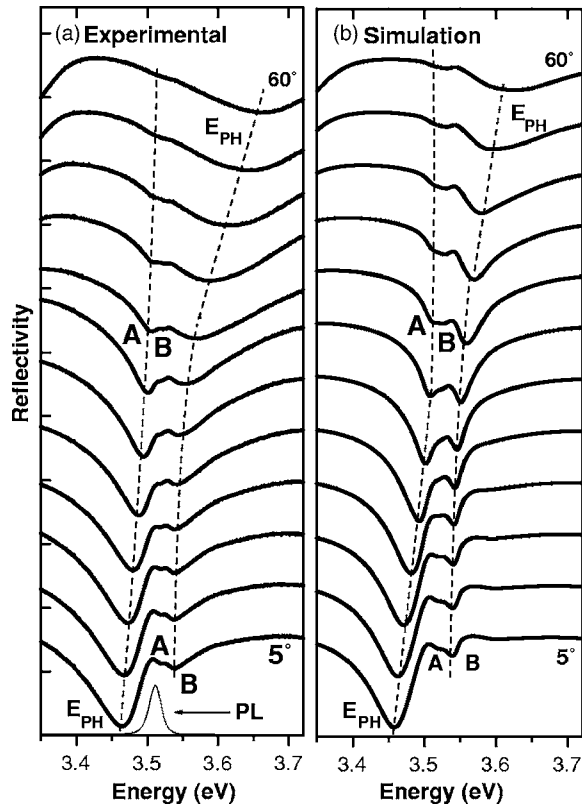


FIG. 1. (a) Experimental angle-resolved reflectivity at 5 K in TE polarization. Also shown is the photoluminescence at 5 K prior to the deposition of the top aluminum mirror. (b) Transfer-matrix simulations at 5 K. The dotted lines are a guide for the eye only. The absence of a dotted line for the central polariton branch is to preserve the clarity of the figure.

threading dislocations, and vertical, due to the progressive relaxation of the compressive strain.<sup>10</sup> As such, we can consider that the 19-meV linewidth of the  $D^0X$  PL line at 5 K is a good estimate for the inhomogeneous broadening in our sample.

The main image in Fig. 1(a) shows the TE-polarized angle-resolved reflectivity at 5 K. For TM-polarized measurements (not shown here) we observed similar features and therefore we concentrate on the TE-polarized measurements only in this article. At an angle of 5° three features are clearly observed in the reflectivity. The optical mode can be observed at  $\sim 3.463$  eV ( $Q \sim 60$ ) negatively detuned with respect to the  $A$  and  $B$  excitonic features observed at 3.521 eV and  $3.533 \pm 0.002$  eV, respectively. The  $A$  and  $B$  excitonic features are also observed in the temperature-dependent photoluminescence spectra (not shown here). The observation of highly resolved  $A$  and  $B$  free excitons in the reflectivity spectra is further evidence of the presence of a large biaxial compression of the GaN film. In  $\mu\text{m}$ -thick GaN on silicon the splitting between  $A$  and  $B$  excitons is of the order of 1 meV and is difficult to observe experimentally.<sup>10</sup> However, compressive strain in GaN acts to increase the degeneracy of the valence bands and results in an ultimate splitting of  $2\Delta_0/3$  between the  $A$  and  $B$  bands, where  $\Delta_0 = 17\text{--}18$  meV (Ref. 13) is the GaN spin-orbit interaction term. This is in rather good agreement with the experimentally observed splitting

between the  $A$ - and  $B$ -excitonic features in Fig. 1(a).

As the angle of incidence is increased, there is a clear anticrossing with a resonance between the  $A$  and  $B$  excitons and the photons at 30° with a  $\Omega_{\text{Rabi}}$  of 50 meV. The difference in oscillator strength of the  $A$  and  $B$  excitons in strongly biaxially compressed GaN at  $k=0$  is weak;<sup>3,13,14</sup> therefore, the coupling between the  $A$  and  $B$  excitons and the optical mode can be assumed to be comparable. The fact that the middle branch in Fig. 1 appears unperturbed by the anticrossing can be understood in terms of its interaction with the other modes of the system. As the three branches interact they create new mixed states which consist of both the excitons and the photon modes. It is through the interaction of these new states that the energy position of the central eigenvalue is set. The maximum shift in energy of this mode is limited by the separation of the  $A$  and  $B$  excitons, in this case  $2\Delta_0/3$ . This property is inherent in  $(3 \times 3)$  matrix analysis where one of the eigenvalues remains approximately constant in relation to the other states of the system.

As the photon passes through the excitonic transitions such that the cavity is positively detuned both excitonic features remain clearly visible. Note also that for energies larger than resonance, the cavity mode strongly broadens, which we attribute to band-to-band absorption in GaN that shortens the photon lifetime. To our knowledge this is the first observation of the strong coupling of both the  $A$  and  $B$  excitons with the photonic mode in a GaN microcavity.

Transfer-matrix reflectivity simulations<sup>14</sup> of the angle-resolved reflectivity are shown in Fig. 1(b). Both  $A$  and  $B$  excitons are included in the simulation with an energy separation of  $15 \pm 2$  meV. The exciton oscillator strengths used are  $35\,000 \pm 5\,000$  meV<sup>2</sup>, consistent with those measured by reflectivity on compressively strained GaN.<sup>13–16</sup> Both homogeneous  $\Gamma$  and inhomogeneous  $\Delta$  broadening are included in the model, with  $\Gamma = 0.1$  meV (Refs. 15 and 16) and  $\Delta = 20$  meV. Furthermore, to account for the experimental Rabi splitting a vertical strain gradient is included in the calculation. To do this, the cavity is simulated as five discrete layers with graded excitonic energies (3 meV), each of these with an inhomogeneous broadening of 15 meV, thus still preserving a total broadening of 20 meV. Note that this value of the inhomogeneous broadening is in good agreement with the estimate taken from the PL. The experimental results are very well reproduced with this analysis. In particular the Rabi energy is well reproduced ( $\sim 50$  meV) and the  $A$  and  $B$  excitons display a clear anticrossing with the photonic mode. It is also evident that the position of the central polariton branch is limited within the energy range determined by the energy separation of the  $A$  and  $B$  excitons.

The interaction between the  $A$  and  $B$  excitons and the photon is illustrated further in Fig. 2. In this figure the energy position of the polariton modes displayed in the angle-dependent reflectivity is plotted as a function of angle and is illustrated as solid triangles (upper polariton branch  $B$ , UPB <sub>$B$</sub> ), squares (upper polariton branch  $A$  and lower polariton branch  $B$ , UPB <sub>$A$</sub>  and LPB <sub>$B$</sub> ), and circles (lower polariton branch  $A$ , LPB <sub>$A$</sub> ), respectively. The subscripts  $A$  and  $B$  indicate the apparent proximity of the feature to the uncoupled  $A$  or  $B$  exciton. The solid lines in the figure indicate the results of a  $(3 \times 3)$  matrix calculation<sup>17</sup> considering the system as an

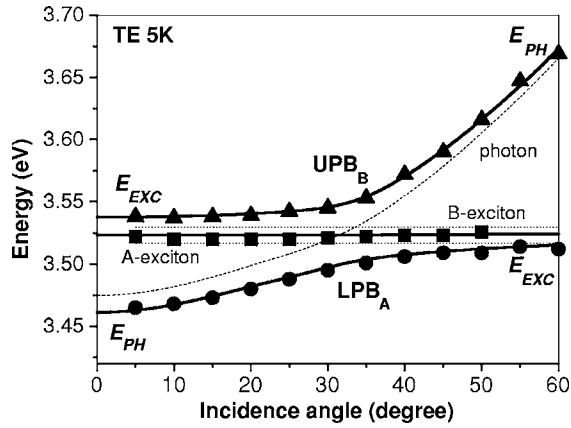


FIG. 2. Variation with angle of incidence of the 5-K polariton modes. Also shown as solid lines are the numerical simulations using  $(3 \times 3)$  matrix analysis of the upper polariton branch,  $UPB_B$  (solid triangles) the coupled upper polariton branch,  $UPB_A$ , and lower polariton branch,  $LPB_B$  (solid squares) and the lower polariton branch,  $LPB_A$  (solid circles). The uncoupled A- and B-excitonic (dashed lines) and photonic modes (dotted line) as a function of angle are also included.

interaction between the A and B excitons with a photon with  $\Omega_{\text{Rabi}} = 54 \pm 3$  meV and  $46 \pm 3$  meV, respectively. The energy of the excitonic A and B transitions is almost independent of angle and is therefore fixed at 3.517 and 3.530 eV while the photon energy is varied as a function of the angle.<sup>18</sup> The C exciton is not considered in the matrix calculations because under biaxial compression it is located at a much higher energy than the A and B excitons and its oscillator strength for near-normal internal incidence is considerably weaker.<sup>3,12,13</sup>

The resulting eigenvalues reproduce the positions of the experimental features very well, indicating that strong coupling occurs via the interaction of both exciton levels with the photons. Also shown in Fig. 2 are the uncoupled A and B excitonic (dotted lines) and the photonic modes (dashed line).

The angle-dependent reflectivity of the microcavity at room temperature is shown in Fig. 3(a). At  $5^\circ$  the photon mode is at  $\sim 3.43$  eV, again negatively detuned from the excitonic features at  $\sim 3.5$  eV, which can no longer be resolved independently due to the effects of thermal broadening. As the angle of incidence is tuned, a clear anticrossing is again observed with a  $\Omega_{\text{Rabi}}$  of  $\sim 50$  meV. The observation of a  $\Omega_{\text{Rabi}}$  of 50 meV at both low to room temperature results from the fact that  $\Omega_{\text{Rabi}} \gg k_B T$ . This is directly related to both the strong oscillator strength and large light-matter interaction length of the bulk GaN active layer in our microcavity.<sup>19</sup> Figure 3(b) shows the transfer-matrix simulation of the microcavity at 300 K, which, again, has very good qualitative agreement with the experimental results. The oscillator strength and energy separation of the A and B excitons are unchanged between 5 and 300 K as the effects of temperature upon both are considered negligible within this range. The homogeneous broadening has been increased to 15 meV.<sup>15,20</sup> The effects of the vertical strain gradient are again included, and though less significant for the simula-

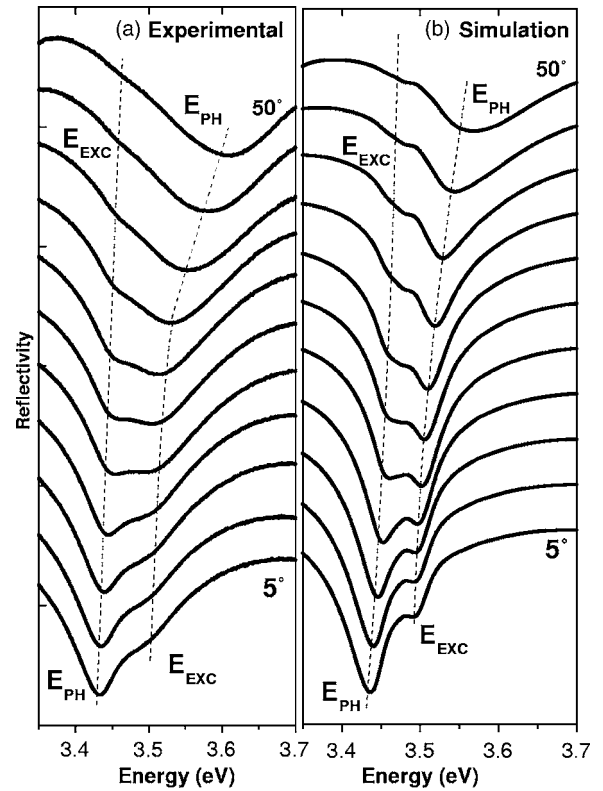


FIG. 3. (a) Experimental angle-resolved reflectivity at 300 K in TE polarization. (b) Transfer-matrix simulations at 300 K. The dotted lines are a guide for the eye only.

tions of the 5 K spectra, it appears necessary for the simulations at 300 K. This illustrates somehow the complicated interplay between inhomogeneous and homogeneous broadening in such a microcavity. At 300 K the thermal broadening of the inhomogeneous linewidth results in the appearance of a single excitonic feature in the reflectivity, reflecting the broadened contribution of both the A and B excitons.<sup>14</sup>

Figure 4 shows the experimental data at room temperature as a function of incidence angle. As an illustration, we also plot the results of a  $(3 \times 3)$  matrix calculation, indicating the interaction of three oscillators, as in the low-temperature case. Using such a  $(3 \times 3)$  matrix analysis the experimental dispersion relation is very well reproduced. In this case the A and B excitons are  $3.477 \pm 0.002$  eV and 3.490 eV, respectively, since the separation between the A and B excitons remains constant between 5 K and room temperature.

It is predicted theoretically that to observe strong coupling in a two-level system the condition  $\Omega_{\text{Rabi}} \gg [\Gamma_{\text{ex}}^2 + \Gamma_{\text{ph}}^2/2]^{1/2}$ , where  $\Gamma_{\text{ex}}$  and  $\Gamma_{\text{ph}}$  are the homogeneous linewidths of the exciton and cavity modes, respectively, must be satisfied.<sup>21</sup> It should be noted here that this equation is related to the energy separation of polariton modes observed in absorption measurements. Although this is not completely consistent with the mode separation measured in reflectivity, the splitting in absorption is always less than that observed in reflectivity;<sup>21</sup> therefore, satisfying this criterion is in fact a more rigorous test of the strong coupling. Actually, since our system is a three-level one, this criterion is not strictly valid.

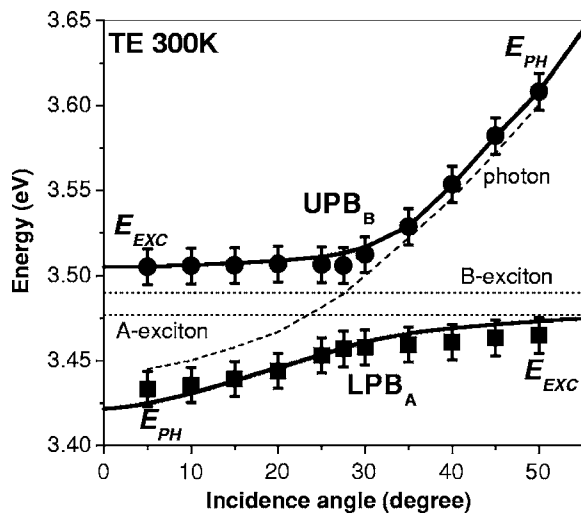


FIG. 4. Variation with angle of incidence of the polariton modes at 300 K. Also shown as a bold lines is the  $(3 \times 3)$  matrix analysis considering the coupling of the photons with both *A*- and *B*-exciton levels. The uncoupled excitonic (dashed lines) and photonic modes (dotted line) as a function of angle are also included in both cases.

However, although the photonic linewidth, related to the optical leakage through the mirrors of the cavity, is large (58 meV), the homogeneous linewidth of the GaN excitons does allow the criteria to be fulfilled. On the other hand, due to the vertical in-plane strain gradient and defect density in

the GaN, the photoluminescence and reflectivity linewidths measured in this work are dominated by inhomogeneous rather than homogeneous broadening. Furthermore, this analysis actually suggests that it is the cavity finesse, rather than the excitonic linewidth, that limits the performance of the microcavity. A factor of 2 improvement of the quality factor is desirable and efforts are currently underway to achieve this.

In summary, we have presented a bulk GaN microcavity structure with epitaxially grown Al(Ga)N DBR's grown directly on silicon. Although there are known to be issues with material quality in such structures,<sup>22</sup> strong light-matter coupling is observed up to room temperature with a  $\Omega_{\text{Rabi}} \sim 50$  meV. At low temperature the interaction between both the free *A*- and *B*-exciton transitions with the photonic mode is clearly resolved. Despite the broadening of the excitonic features, transfer-matrix reflectivity simulations suggest that the overall  $\Omega_{\text{Rabi}}$  still results from the contribution from both the *A*- and *B*-excitonic transitions at room temperature.

The authors would like to acknowledge the contribution to this work of Denis Lefevbre (CRHEA-CNRS) with regard to the optimization of our molecular beam epitaxy reactor control system and Jean-Yves Duboz for stimulating discussions. We would also like to acknowledge the European community for funding through the EC-RTN "CLERMONT2" program, Contract No. MRTN-CT-2003-503667.

\*Electronic address: is@crhea.cnrs.fr

- <sup>1</sup>C. Weisbuch, M. Nishioka, A. Ishikawa, and Y. Arakawa, *Phys. Rev. Lett.* **69**, 3314 (1992).
- <sup>2</sup>M. S. Skolnick, T. A. Fisher, and D. M. Whittaker, *Semicond. Sci. Technol.* **13**, 645 (1998).
- <sup>3</sup>J. J. Hopfield, *Phys. Rev.* **112**, 1555 (1958).
- <sup>4</sup>M. Saba, C. Cuiti, J. Bloch, V. Thierry-Mieg, R. André, Le Si Dang, S. Kundermann, A. Mura, G. Bioniovanni, J. L. Stadelhli, and B. Deveaud, *Nature (London)* **414**, 731 (2001).
- <sup>5</sup>P. G. Savvidis, J. J. Baumberg, R. M. Stevenson, M. S. Skolnick, D. M. Whittaker, and J. S. Roberts, *Phys. Rev. Lett.* **84**, 1547 (2000).
- <sup>6</sup>A. Kavokin and B. Gil, *Appl. Phys. Lett.* **72**, 2880 (1998).
- <sup>7</sup>N. Antoine-Vincent, F. Natali, D. Byrne, A. Vasson, P. Disseix, J. Leymarie, M. Leroux, F. Semond, and J. Massies, *Phys. Rev. B* **68**, 153313 (2003).
- <sup>8</sup>F. Semond, I. R. Sellers, F. Natali, D. Byrne, M. Leroux, J. Massies, N. Ollier, J. Leymarie, P. Disseix, and A. Vasson, *Appl. Phys. Lett.* **87**, 021102 (2005).
- <sup>9</sup>T. Tawara, H. Gotoh, T. Akasaka, N. Kobayashi, and T. Saitoh, *Phys. Rev. Lett.* **92**, 256402 (2004).
- <sup>10</sup>F. Semond, B. Damilano, S. Vézian, N. Grandjean, M. Leroux, and J. Massies, *Phys. Status Solidi B* **216**, 101 (1999).
- <sup>11</sup>M. Leroux, N. Grandjean, B. Beaumont, G. Nataf, F. Semond, J. Massies, and P. Gibart, *J. Appl. Phys.* **86**, 3721 (1999).

- <sup>12</sup>H. Lahrèche, M. Leroux, M. Laügt, M. Vaille, B. Beaumont, and P. Gibart, *J. Appl. Phys.* **87**, 577 (2000).
- <sup>13</sup>B. Gil and O. Briot, *Phys. Rev. B* **55**, 2530 (1997).
- <sup>14</sup>N. Ollier, F. Natali, D. Bryne, P. Disseix, M. Mihailovic, A. Vasson, J. Leymarie, F. Semond, and J. Massies, *Jpn. J. Appl. Phys., Part 1* **44**, 4902 (2005).
- <sup>15</sup>L. Sizade, S. Colard, M. Mihailovic, J. Leymarie, A. Vasson, N. Grandjean, M. Leroux, and J. Massies, *Jpn. J. Appl. Phys., Part 1* **39**, 20 (2000).
- <sup>16</sup>O. Aoudé, P. Disseix, J. Leymarie, A. Vasson, E. Aujol, and B. Beaumont, *Superlattices Microstruct.* **36**, 607 (2004).
- <sup>17</sup>S. Pau, G. Bjork, J. Jacobson, H. Cao, and Y. Yamamoto, *Phys. Rev. B* **51**, 14437 (1996).
- <sup>18</sup>D. Baxter, M. S. Skolnick, A. Armitage, V. N. Astratov, D. M. Whittaker, T. A. Fisher, J. S. Roberts, D. J. Mowbray, and M. A. Kaliteevski, *Phys. Rev. B* **56**, R10032 (1997).
- <sup>19</sup>A. Tredicucci, Y. Chen, V. Pellegrini, and C. Deparis, *Appl. Phys. Lett.* **66**, 2388 (1995).
- <sup>20</sup>M. Zamfirescu, B. Gil, N. Grandjean, G. Malpuech, A. Kavokin, P. Bigenwald, and J. Massies, *Phys. Rev. B* **64**, 121304(R) (2001).
- <sup>21</sup>V. Savona, L. C. Andreani, P. Schwendimann, and A. Quattropani, *Solid State Commun.* **93**, 733 (1995).
- <sup>22</sup>F. Natali, D. Byrne, A. Dussaigne, N. Grandjean, and J. Massies, *Appl. Phys. Lett.* **82**, 509 (2003).